

## GALACTIC $^{12}\text{C}/^{13}\text{C}$ RATIOS FROM MILLIMETER-WAVE OBSERVATIONS OF INTERSTELLAR CN

C. SAVAGE,<sup>1</sup> A. J. APPONI,<sup>2</sup> AND L. M. ZIURYS

Department of Chemistry, Department of Astronomy, and Steward Observatory, University of Arizona,  
933 North Cherry Avenue, Tucson, AZ 85721

AND

S. WYCKOFF

Department of Physics and Astronomy, Arizona State University, Tempe, AZ 85287

Received 2002 March 18; accepted 2002 June 20

### ABSTRACT

The  $N = 1 \rightarrow 0$  transitions of  $^{12}\text{CN}$  and  $^{13}\text{CN}(X^2\Sigma^+)$  at 113.5 and 108.8 GHz, respectively, have been observed in a sample of 13 Galactic molecular clouds using the Kitt Peak 12 m radio telescope. The objects studied include the Galactic center [SgrB2(OH)], sources in the solar neighborhood such as Orion A and NGC 2024, and various other clouds with and without star formation. Hyperfine structure, arising from the nitrogen nuclear spin, was resolved in the spectra of both species, enabling an accurate determination of the opacity in  $^{12}\text{CN}$ . From these measurements, estimates of the  $^{12}\text{C}/^{13}\text{C}$  isotope ratio were obtained. These values fall in the range  $^{12}\text{C}/^{13}\text{C} \sim 20\text{--}70$  and exhibit a noticeable gradient with distance from the Galactic center. In general, the ratios obtained from CN are very similar to those determined from millimeter observations of CO but are consistently lower than those derived from  $\text{H}_2\text{CO}$ . If chemical fractionation is occurring in CN, it is comparable to that in CO. The highest  $^{12}\text{C}/^{13}\text{C}$  ratios ( $65 \pm 12$  and  $70 \pm 11$ ) were obtained toward two known photon-dominated regions (the Orion Bar and NGC 2024); CN in these two sources may be undergoing some isotope-selective photodissociation. The  $^{12}\text{C}/^{13}\text{C}$  ratio of  $43 \pm 7$ , found in Orion A, is similar to that determined from optical observations of CN toward a nearby source,  $\zeta$  Ophiuchi, but significantly lower than the average value found in comets ( $90 \pm 10$ ). This difference suggests that substantial enrichment of  $^{13}\text{C}$  has occurred during the past 4.6 Gyr in the solar neighborhood.

*Subject headings:* astrochemistry — Galaxy: abundances — ISM: abundances — ISM: clouds — ISM: molecules — radio lines: ISM

### 1. INTRODUCTION

The  $^{12}\text{C}/^{13}\text{C}$  isotope ratio in interstellar gas is thought to be a sensitive indicator of the degree of stellar nucleosynthesis and therefore Galactic chemical evolution. Carbon-12 is produced predominantly in helium burning via the  $3\alpha$  reaction, considered to be a primary nucleosynthetic process (Woosley & Weaver 1995). In contrast,  $^{13}\text{C}$  is formed from  $^{12}\text{C}$  with some equilibrium concentration during the catalytic CNO cycle, which also destroys it, making this isotope a product of secondary processes. The CNO cycle occurs primarily in the red giant/supergiant phases, and the  $^{13}\text{C}$  abundance is partially preserved because of dredge-up mechanisms (Blöcker 1999). It is thought that as more stars form, the contribution of secondary processes in nucleosynthesis increases relative to primary ones. Consequently, as the Galaxy evolves, more  $^{13}\text{C}$  should be produced relative to  $^{12}\text{C}$ , lowering the  $^{12}\text{C}/^{13}\text{C}$  ratio (Timmes, Woosley, & Weaver 1995).

Measurements of this important isotope ratio have been carried out for many years across the Galaxy, using both radio and optical spectral measurements. In general, the carbon ratio has been obtained by observing  $^{12}\text{C}$  and  $^{13}\text{C}$  molecular isotopomers in diffuse and dense clouds. Optically, such measurements include  $\text{CH}^+$  (see, e.g., Hawkins, Craig, & Meyer 1993; Centurión, Càssola, & Vladilo 1995), CN (Kaiser, Wright, & Hawkins 1991; Roth & Meyer

1995), and CO (Lambert et al. 1994). In the radio/millimeter regions, CO (Langer & Penzias 1990, 1993) and  $\text{H}_2\text{CO}$  (Henkel, Güsten, & Gardner 1985; Henkel, Wilson, & Bieging 1982) are the major sources of  $^{12}\text{C}/^{13}\text{C}$  ratios. Very recently, submillimeter observations of neutral carbon and  $\text{C}^+$  fine-structure lines (Keene et al. 1998; Boreiko & Betz 1996) have additionally been used as ratio indicators.

None of these tracers, however, are particularly ideal. Optical measurements of  $^{13}\text{C}$  isotopomers are typically limited by poor signal-to-noise ratio (Hawkins et al. 1993). Radio lines are stronger and better resolved, but the  $^{12}\text{C}$  species are usually very abundant and hence exhibit transitions that have high opacities. Such opacities are difficult to evaluate, and thus  $^{12}\text{C}/^{13}\text{C}$  ratios obtained are often underestimated. Consequently, for CO, double ratios involving  $\text{C}^{18}\text{O}$  are used (see Wilson 1999 for a discussion), or, as for  $\text{H}_2\text{CO}$ , LVG modeling is employed for opacity estimates. All molecular measurements also may be subject to chemical fractionation, resulting from the fact that the  $^{13}\text{C}$  isotopomer has a slightly lower zero-point energy, favoring this species over its  $^{12}\text{C}$  counterpart (Watson, Anicich, & Huntress 1976). Another effect is isotope-selective photodissociation, which, in regions of high UV flux, favors the more abundant  $^{12}\text{C}$  isotope because of self-shielding (van Dishoeck & Black 1988). Other ratio-altering phenomena such as “ $^{13}\text{C}$  starvation” are possible as well (Langer et al. 1984; Lucas & Liszt 1998). Naturally, direct measurements of C and  $\text{C}^+$  are intrinsically more reliable, but observations of these fine-structure lines are difficult because of atmospheric conditions at submillimeter/far-IR wavelengths.

<sup>1</sup> NASA Graduate Student Research Program Fellow.

<sup>2</sup> DeFrancis Fellow, National Italian-American Foundation.

Nonetheless, many Galactic measurements of the  $^{12}\text{C}/^{13}\text{C}$  ratio have been conducted using these molecular tracers. As summarized by Wilson & Rood (1994) and Wilson (1999), the ratios vary from as low as  $^{12}\text{C}/^{13}\text{C} \sim 20$  at the Galactic center to values greater than 100 at distances of 8–10 kpc from the center. The local ISM value is  $69 \pm 6$ . Thus, there appears to be a distinct gradient to this ratio with Galactic center distance. Moreover, it has been found that values obtained from  $\text{H}_2\text{CO}$  are usually higher than those derived from CO. This difference is thought to occur because highly stable  $^{13}\text{CO}$  serves as an effective reservoir for carbon-13 (Langer et al. 1984). Finally, local ISM values vary significantly from the solar system ratio of 89 (Anders & Grevesse 1989). The ratios are thought to disagree because the solar isotope value reflects conditions in the interstellar medium at an earlier epoch (see, e.g., Wyckoff et al. 2000).

In an effort to better establish  $^{12}\text{C}/^{13}\text{C}$  ratios throughout the Galaxy, as well as understand the chemistry of isotopic fractionation, we have conducted millimeter observations of another molecular tracer of this quantity: CN. This species was chosen because it exhibits appreciable hyperfine (hf) structure. (It is a radical with a  $^2\Sigma^+$  ground electronic state and contains a nitrogen atom, which has a nuclear spin of  $I = 1$ .) Consequently, rotational transitions of CN are split into hf components from which opacities and abundances can be accurately evaluated. In addition, CN is sufficiently prevalent in molecular clouds such that its  $^{13}\text{CN}$  isotopomer is generally detectable. CN therefore offers a means to establish  $^{12}\text{C}/^{13}\text{C}$  ratios without the use of double isotope measurements or model-dependent opacity determinations.

To obtain carbon isotope ratios, the  $N = 1 \rightarrow 0$  transitions of  $^{12}\text{CN}$  and  $^{13}\text{CN}$  were observed at 113 and 108 GHz, respectively, using the Kitt Peak 12 m telescope. A sample of molecular clouds was studied, including several star-forming regions. A range of opacities was found for  $^{12}\text{CN}$ , necessitating an accurate evaluation of the optical depth effects in the calculation of the  $^{12}\text{C}/^{13}\text{C}$  ratios. Here we present our results, compare them with previous carbon isotope ratios, and discuss these data in the context of chemical fractionation, isotope-selective photodissociation, and the chemical evolution of the Galaxy.

## 2. QUANTUM MECHANICS OF THE CN RADICAL ( $X^2\Sigma^+$ )

$^{12}\text{CN}$  and  $^{13}\text{CN}$  are both free radicals with one unpaired electron in a  $\sigma$  orbital, which gives rise to a  $^2\Sigma^+$  ground electronic state. As with most  $^2\Sigma$  molecules, the spectrum of  $^{12}\text{CN}$  is best described by a Hund's case  $b_{\beta J}$  coupling scheme. For such coupling, the electron spin angular momentum  $\mathbf{S}$  adds to the molecular frame rotation  $\mathbf{N}$  ( $=\mathbf{R}$ ) to generate a total angular momentum  $\mathbf{J}$  (neglecting nuclear effects), namely,  $\mathbf{N} + \mathbf{S} = \mathbf{J}$ . This coupling results in two fine-structure levels per rotational transition. The nuclear spin angular momentum of the nitrogen atom  $\mathbf{I}$  then couples with  $\mathbf{J}$  to form a total angular momentum  $\mathbf{F}$ , where  $\mathbf{F} = \mathbf{I} + \mathbf{J}$ . This splits each fine-structure doublet further into hf levels. The quantum number labeling for each energy level in  $^{12}\text{CN}$  therefore concerns  $N$ ,  $J$ , and  $F$ , and selection rules for electric-dipole allowed transitions are  $\Delta N = \pm 1$ ,  $\Delta J = 0, \pm 1$ , and  $\Delta F = 0, \pm 1$  ( $0 \not\leftrightarrow 0$ ).

The quantum mechanical structure of  $^{13}\text{CN}$  is more complicated because, in addition to the nitrogen spin, the  $^{13}\text{C}$  nucleus is present. This nucleus also has a spin ( $I = \frac{1}{2}$ ), which couples to the rotational and electron spin angular momenta (Bogey, Demuyneck, & Destombes 1984). The coupling scheme that best describes the spectrum of  $^{13}\text{CN}$  is a combination of Hund's cases  $b_{\beta J}$  and  $b_{\beta S}$ . In this scenario, the electron spin first couples with the  $^{13}\text{C}$  nuclear spin ( $\mathbf{S} + \mathbf{I}_1 = \mathbf{F}_1$ ), as in the  $b_{\beta S}$  case. The molecular frame rotation  $\mathbf{N}$  then adds to  $\mathbf{F}_1$  to form angular momentum  $\mathbf{F}_2$ , which subsequently couples with the second nuclear spin from the nitrogen atom  $\mathbf{I}_2$  to generate the total angular momentum  $\mathbf{F}$ , i.e.,  $\mathbf{N} + \mathbf{F}_1 = \mathbf{F}_2$  and  $\mathbf{F}_2 + \mathbf{I}_2 = \mathbf{F}$ —closer to  $b_{\beta J}$  coupling. Quantum numbers  $N$ ,  $F_1$ ,  $F_2$ , and  $F$  are thus required to label all energy levels of  $^{13}\text{CN}$ , and the selection rules on  $F_1$  and  $F_2$  are  $\Delta F_1 = 0, \pm 1$  and  $\Delta F_2 = 0, \pm 1$ .

## 3. OBSERVATIONS

The measurements were carried out in several observing sessions during the period from 1996 June to 2002 January using the former National Radio Astronomy Observatory (NRAO)<sup>3</sup> 12 m telescope at Kitt Peak, Arizona.<sup>4</sup> The observing frequency used for the  $N = 1 \rightarrow 0$  transition of  $^{12}\text{CN}$  was 113,490.985 MHz and that used for  $^{13}\text{CN}$  was 108,782.374 MHz. The beam sizes at these frequencies are estimated to be  $59''$  and  $58''$ , while the main-beam efficiencies  $\eta_c$  are 0.82 and 0.84. The receiver used was a dual-channel, cooled SIS mixer, operated in single-sideband mode with about 20 dB image rejection. The temperature scale was determined by the chopper wheel method, corrected for forward spillover losses, and is given in terms of  $T_R^*$ , where  $T_R = T_R^*/\eta_c$ . The back ends used were two 256 channel filter banks with different spectral resolutions configured in parallel mode ( $2 \times 128$  channels) for the two receiver channels. Typically, the 250/500 kHz resolution combination was employed for most molecular clouds, although 1000/2000 and 100/250 kHz combinations were also used for certain very warm or very cold objects. The millimeter autocorrelator was also employed for an additional back end with spectral resolutions ranging from 24 to 768 kHz. All data were taken in position-switching mode, with the off position  $30'$  west in azimuth and a switching rate of 15 s. Pointing was established by observations of planets and quasars.

The  $N = 1 \rightarrow 0$ ,  $J = 3/2 \rightarrow 1/2$  transition of  $^{12}\text{CN}$  consists of two spin-rotation components, sufficiently separated in frequency such that only one component can be observed at a time. The stronger doublet,  $J = 3/2 \rightarrow 1/2$ , was chosen for measurements; it consists of five hf components, separated by a total of 32 MHz, which comprise two-thirds of the intensity of the  $N = 1 \rightarrow 0$  transition, as shown in Table 1. The strongest hf component,  $F = 5/2 \rightarrow 3/2$ , contains 33% of the total intensity. Using the frequency of this line (113,490.98 MHz) as the center, all five hf components could be observed simultaneously in the 500 kHz or 1 MHz filter banks. This situation was the setup for most of the sources observed, except for the dark clouds.

<sup>3</sup> NRAO is operated by the Associated Universities, Inc., under cooperative agreement with the National Science Foundation.

<sup>4</sup> The Kitt Peak 12 m telescope is currently operated by Steward Observatory (University of Arizona), with support from the National Science Foundation and the Research Corporation.

TABLE 1  
FREQUENCIES AND RELATIVE INTENSITIES OF THE OBSERVED HYPERFINE  
COMPONENTS OF CN AND  $^{13}\text{CN}$

Isotopomer	Transition	Component	Frequency (MHz)	Relative Intensity
$^{12}\text{CN}^{\text{a}}$ .....	$N = 1 \rightarrow 0$ $J = 3/2 \rightarrow 1/2$	$F = 3/2 \rightarrow 1/2$	113488.142	0.1235
		$F = 5/2 \rightarrow 3/2$	113490.985	0.3333
		$F = 1/2 \rightarrow 1/2$	113499.643	0.0988
		$F = 3/2 \rightarrow 3/2$	113508.934	0.0988
		$F = 1/2 \rightarrow 3/2$	113520.414	0.0123
$^{13}\text{CN}^{\text{b}}$ .....	$N = 1 \rightarrow 0$ $F_2 = 2 \rightarrow 1$	$F = 3 \rightarrow 2$	108780.201	0.200
		$F = 2 \rightarrow 1$	108782.374	0.107
		$F = 2 \rightarrow 2$	108796.400	0.036
		$F = 1 \rightarrow 1$	108793.753	0.036
		$F = 1 \rightarrow 0$	108786.982	0.048

<sup>a</sup> From Skatrud et al. 1983.

<sup>b</sup> From Bogey et al. 1984.

The  $N = 1 \rightarrow 0$  transition of  $^{13}\text{CN}$ , in contrast, consists of four groups of hf lines indicated by quantum number  $F_2$  ( $F_2'' \rightarrow F_2' = 0 \rightarrow 1, 1 \rightarrow 2, 1 \rightarrow 1$ , and  $1 \rightarrow 0$ ; see Bogey et al. 1984). The strongest hf line is the  $F_2 = 2 \rightarrow 1, F = 3 \rightarrow 2$  component at 108,780.2 MHz (see Table 1), which contributes 20% of the total intensity of the transition. Four other hf lines lie within 16 MHz of the  $F = 3 \rightarrow 2$  transition but are considerably weaker. Again, it was possible to observe all five hf lines simultaneously in the 500 kHz or 1 MHz filters.

A total of 13 molecular clouds were observed in  $^{12}\text{CN}$  and  $^{13}\text{CN}$ . The sources and their coordinates are listed in Table 2. Typical integration times were 1–2 hr for  $^{12}\text{CN}$  and 4–12 hr for  $^{13}\text{CN}$ .

#### 4. RESULTS

The  $^{12}\text{CN}$  and  $^{13}\text{CN}$  measurements are summarized in Table 2, where the antenna temperatures, LSR velocities, and line widths are given for all detected hf components. These parameters, and their errors, were determined by Gaussian fits to the line profiles. In general, both  $^{12}\text{CN}$  and  $^{13}\text{CN}$  were detected in all sources except L134N, where the  $^{13}\text{CN}$  isotopomer was only tentatively observed. Also, all five hf lines of  $^{12}\text{CN}$  ( $J = 3/2 \rightarrow 1/2$  component) were detected in clouds where larger bandwidths could be used, with the exception of W49 and Orion A. In these objects, the weak  $F = 1/2 \rightarrow 3/2$  component (1.23% total intensity) was not observed. Two sources had  $^{12}\text{CN}$  spectra that showed evidence of self-reversal [DR-21(OH) and SgrB2(OH)], and one source, W49, had data consisting of two velocity components. Toward L134N and TMC-1, only the two strongest hf lines of  $^{12}\text{CN}$  were present in the narrow bandpass necessary for these sources; both were observed.

For  $^{13}\text{CN}$ , usually only the two strongest hf components,  $F = 3 \rightarrow 2$  and  $F = 2 \rightarrow 1$ , were detected in most objects. They are 2 MHz apart in frequency and so were often blended together. However, toward DR-21(OH), SgrB2(OH), and W3(OH), additional, weaker  $^{13}\text{CN}$  hf lines were also visible in the data.

The spectra of both  $^{12}\text{CN}$  and  $^{13}\text{CN}$  for each source are presented in Figures 1a–1m. Here some interesting effects are visible. For about one-third of the objects, the  $^{12}\text{CN}$

lines appear to be optically thin and follow the

$$\begin{aligned}
 F = 5/2 \rightarrow 3/2 : 3/2 \rightarrow 1/2 : 1/2 \rightarrow 1/2 : \\
 3/2 \rightarrow 3/2 : 1/2 \rightarrow 3/2 \\
 = 0.33 : 0.12 : 0.099 : 0.099 : 0.012
 \end{aligned}$$

intensity pattern. Good examples are Orion A and the Orion Bar (see Figs. 1f and 1k). In most of the objects studied, however, the  $^{12}\text{CN}$ ,  $N = 1 \rightarrow 0$  transition appears to be somewhat optically thick, as indicated by stronger  $F = 3/2 \rightarrow 1/2, 1/2 \rightarrow 1/2$ , and  $3/2 \rightarrow 3/2$  components relative to the main line. Sources where larger opacities are clearly present are NGC 2024 (Orion B) and NGC 7538 (Figs. 1a and 1h). In some sources, the  $F = 1/2 \rightarrow 1/2$  component appears anomalously weak, in particular W33 and G34.3 (Figs. 1i and 1e). In fact, the intensity ratio of this line to the main line is not consistent with intensity ratios of other components. This effect could result from subtle differences in collisional cross sections for the hf levels as a function of temperature but needs further investigation. An even more pronounced non-LTE ratio is observed in the  $^{12}\text{CN}$  spectrum of TMC-1, where the weaker  $3/2 \rightarrow 1/2$  component is stronger than the  $5/2 \rightarrow 3/2$  line (see Fig. 1m). In the limit of very large optical depths, as observed in L134N, the  $F = 3/2 \rightarrow 1/2$  line should be equal in intensity to the main component (Fig. 1l) but not stronger.

The  $^{13}\text{CN}$  spectrum obtained toward DR-21(OH) is clear evidence that the absorption “dips” in the  $^{12}\text{CN}$  data arise from self-reversal (Fig. 1d). Certainly such self-reversal has been observed in other molecules of comparable abundance to CN in this cloud (see Richardson et al. 1986). Figure 1c shows the W49 data; the double-peaked profiles in  $^{12}\text{CN}$  in this case can be attributed to two distinct velocity components near 4 and 12 km s<sup>-1</sup>, which probably are also present in the  $^{13}\text{CN}$  data. The presence of these two components has been recognized in  $\text{N}_2\text{H}^+$  and other molecules (see, e.g., Womack, Ziurys, & Wyckoff 1992). Finally, the SgrB2(OH),  $^{12}\text{CN}$  spectrum, presented in Figure 1j, exhibits strong features not present at the typical hf frequencies. The anomalous positions of the  $^{12}\text{CN}$  lines likely arise because of the superposition of absorption and emission features of the stronger hf components. In the  $^{13}\text{CN}$  data, a strong absorption feature exists near the frequency of the main hf line. However, all the other  $^{13}\text{CN}$  components appear as

TABLE 2  
OBSERVATIONS OF  $^{12}\text{CN}$  ( $N = 1 \rightarrow 0, J = 3/2 \rightarrow 1/2$ ) AND  $^{13}\text{CN}$  ( $N = 1 \rightarrow 0, F_2 = 2 \rightarrow 1$ ) TOWARD MOLECULAR CLOUDS

Source	$\alpha$ (B1950.0)	$\delta$ (B1950.0)	Isotopomer	hf Component	$T_R^*$ (K)	$\Delta V_{1/2}$ (km s $^{-1}$ )	$V_{\text{LSR}}$ (km s $^{-1}$ )
W3(OH) <sup>a</sup> .....	02 23 17.0	61 38 54	CN	$F = 3/2 \rightarrow 1/2$	$0.65 \pm 0.02$	$5.1 \pm 0.2$	$-47.9 \pm 0.4$
				$F = 5/2 \rightarrow 3/2$	$1.36 \pm 0.02$	$4.6 \pm 0.1$	$-48.0 \pm 0.4$
				$F = 1/2 \rightarrow 1/2$	$0.42 \pm 0.02$	$4.1 \pm 0.2$	$-47.9 \pm 0.4$
				$F = 3/2 \rightarrow 3/2$	$0.54 \pm 0.02$	$4.6 \pm 0.2$	$-47.8 \pm 0.4$
				$F = 1/2 \rightarrow 3/2$	$\sim 0.08$	$\sim 7.8$	$\sim -48$
W49 <sup>a,b</sup> .....	19 07 49.8	09 01 17	CN	$F = 3 \rightarrow 2$	$0.030 \pm 0.004$	$3.7 \pm 0.5$	$-47.1 \pm 1.1$
				$F = 2 \rightarrow 1$	$0.016 \pm 0.004$	$5.1 \pm 1.3$	$-47.1 \pm 1.0$
				$F = 3/2 \rightarrow 1/2$	$1.35 \pm 0.01^c$	$\sim 5$	$\sim 3.3$
				$F = 5/2 \rightarrow 3/2$	$1.44 \pm 0.01$	$8.0 \pm 0.5$	$3.5 \pm 0.1$
				$F = 1/2 \rightarrow 1/2$	$0.26 \pm 0.02$	$7.0 \pm 1.7$	$3.6 \pm 0.1$
DR-21(OH) <sup>a,d</sup> .....	20 37 14.0	42 12 00	CN	$F = 3/2 \rightarrow 1/2$	$1.45 \pm 0.04^d$	$2.5 \pm 0.1$	$-3.1 \pm 1.2$
				$F = 5/2 \rightarrow 3/2$	$2.86 \pm 0.02^d$	$2.8 \pm 0.1$	$-3.0 \pm 1.3$
				$F = 1/2 \rightarrow 1/2$	$0.87 \pm 0.03^d$	$2.8 \pm 0.1$	$-3.3 \pm 1.0$
				$F = 3/2 \rightarrow 3/2$	$1.17 \pm 0.03^d$	$3.0 \pm 0.2$	$-3.3 \pm 1.0$
				$F = 1/2 \rightarrow 3/2$	$0.25 \pm 0.03^d$	$3.5 \pm 0.2$	$-3.2 \pm 0.2$
G34.3 <sup>a</sup> .....	18 50 46.4	01 11 14	CN	$F = 3 \rightarrow 2$	$0.114 \pm 0.010$	$3.8 \pm 0.3$	$-3.2 \pm 0.2$
				$F = 2 \rightarrow 1$	$0.069 \pm 0.010$	$2.8 \pm 0.3$	$-3.1 \pm 0.2$
				$F = 1 \rightarrow 0$	$0.027 \pm 0.010$	$3.4 \pm 0.4$	$-2.9 \pm 0.4$
				$F = 3/2 \rightarrow 1/2$	$0.90 \pm 0.08$	$2.9 \pm 0.4$	$57.2 \pm 0.8$
				$F = 5/2 \rightarrow 3/2$	$1.73 \pm 0.07$	$3.6 \pm 0.2$	$56.2 \pm 0.9$
Orion A <sup>a</sup> .....	05 32 46.8	-05 24 23	CN	$F = 1/2 \rightarrow 1/2$	$0.39 \pm 0.07$	$3.7 \pm 0.6$	$56.5 \pm 0.7$
				$F = 3/2 \rightarrow 3/2$	$0.67 \pm 0.07$	$3.7 \pm 0.3$	$56.8 \pm 0.8$
				$F = 1/2 \rightarrow 3/2$	$\leq 0.15$	...	...
				$F = 3 \rightarrow 2$	$0.12 \pm 0.02$	$3.7 \pm 0.5$	$58.0 \pm 0.4$
				$F = 2 \rightarrow 1$	$\sim 0.06$	$\sim 4.2$	$\sim 58$
W51M <sup>a</sup> .....	19 21 26.2	14 24 43	CN	$F = 3/2 \rightarrow 1/2$	$1.47 \pm 0.03$	$4.2 \pm 0.1$	$8.5 \pm 0.5$
				$F = 5/2 \rightarrow 3/2$	$4.17 \pm 0.03$	$3.7 \pm 0.1$	$8.6 \pm 0.4$
				$F = 1/2 \rightarrow 1/2$	$0.95 \pm 0.03$	$3.4 \pm 0.1$	$8.7 \pm 0.3$
				$F = 3/2 \rightarrow 3/2$	$1.00 \pm 0.03$	$3.7 \pm 0.1$	$8.6 \pm 0.4$
				$F = 1/2 \rightarrow 3/2$	$\leq 0.13$	...	...
NGC 7538 <sup>a</sup> .....	23 11 36.6	61 11 47	CN	$F = 3 \rightarrow 2$	$0.060 \pm 0.009$	$3.9 \pm 0.01$	$8.6 \pm 0.4$
				$F = 2 \rightarrow 1$	$0.027 \pm 0.009$	$3.8 \pm 0.01$	$8.4 \pm 0.6$
				$F = 3/2 \rightarrow 1/2$	$3.14 \pm 0.05^e$	$10.3 \pm 0.1$	$\sim 56$
				$F = 5/2 \rightarrow 3/2$			
				$F = 1/2 \rightarrow 1/2$	$0.77 \pm 0.05$	$9.2 \pm 0.5$	$56.2 \pm 0.2$
NGC 2024 <sup>a</sup> .....	05 39 13.0	-01 57 04	CN	$F = 3/2 \rightarrow 3/2$	$1.10 \pm 0.05$	$9.4 \pm 0.4$	$56.5 \pm 0.3$
				$F = 1/2 \rightarrow 3/2$	$0.16 \pm 0.05$	$9.2 \pm 0.5$	$55.8 \pm 0.4$
				$F = 3 \rightarrow 2$	$0.089 \pm 0.004^e$	$10.2 \pm 0.5$	$57.4 \pm 0.4$
				$F = 2 \rightarrow 1$			
				$F = 3/2 \rightarrow 1/2$	$1.01 \pm 0.03$	$5.5 \pm 0.2$	$-57.3 \pm 0.7$
W33 <sup>f</sup> .....	18 11 19.5	-17 57 14	CN	$F = 5/2 \rightarrow 3/2$	$1.98 \pm 0.03$	$4.5 \pm 0.1$	$-57.5 \pm 0.7$
				$F = 1/2 \rightarrow 1/2$	$0.59 \pm 0.03$	$4.8 \pm 0.2$	$-57.1 \pm 0.5$
				$F = 3/2 \rightarrow 3/2$	$0.72 \pm 0.03$	$4.9 \pm 0.2$	$-57.1 \pm 0.5$
				$F = 1/2 \rightarrow 3/2$	$0.12 \pm 0.04$	$4.1 \pm 1.1$	$-57.1 \pm 0.6$
				$F = 3 \rightarrow 2$	$0.044 \pm 0.004$	$4.1 \pm 0.4$	$-57.3 \pm 0.7$
W33 <sup>f</sup> .....	18 11 19.5	-17 57 14	CN	$F = 2 \rightarrow 1$	$\sim 0.01$	$\sim 4$	$\sim -57$
				$F = 3/2 \rightarrow 1/2$	$1.82 \pm 0.04$	$2.9 \pm 0.1$	$11.3 \pm 0.2$
				$F = 5/2 \rightarrow 3/2$	$3.08 \pm 0.04$	$3.1 \pm 0.1$	$11.1 \pm 0.04$
				$F = 1/2 \rightarrow 1/2$	$1.43 \pm 0.04$	$2.9 \pm 0.1$	$11.2 \pm 0.1$
				$F = 3/2 \rightarrow 3/2$	$1.52 \pm 0.04$	$3.1 \pm 0.1$	$11.3 \pm 0.2$
W33 <sup>f</sup> .....	18 11 19.5	-17 57 14	CN	$F = 1/2 \rightarrow 3/2$	$0.27 \pm 0.04$	$3.2 \pm 0.4$	$11.7 \pm 0.6$
				$F = 3 \rightarrow 2$	$0.098 \pm 0.02$	$2.6 \pm 0.4$	$11.3 \pm 0.2$
				$F = 2 \rightarrow 1$	$0.050 \pm 0.03$	$1.7 \pm 0.9$	$11.5 \pm 0.4$
				$F = 3/2 \rightarrow 1/2$	$1.23 \pm 0.03$	$5.1 \pm 0.07$	$36.4 \pm 1.5$
				$F = 5/2 \rightarrow 3/2$	$2.62 \pm 0.03$	$6.6 \pm 0.04$	$35.6 \pm 1.2$
W33 <sup>f</sup> .....	18 11 19.5	-17 57 14	CN	$F = 1/2 \rightarrow 1/2$	$0.46 \pm 0.03$	$6.6 \pm 0.2$	$36.5 \pm 1.6$
				$F = 3/2 \rightarrow 3/2$	$0.95 \pm 0.03$	$6.6 \pm 0.09$	$35.9 \pm 1.2$
				$F = 1/2 \rightarrow 3/2$	$0.19 \pm 0.04$	$5.4 \pm 0.5$	$35.8 \pm 1.4$
				$F = 3 \rightarrow 2$	$0.089 \pm 0.02^e$	$9.4 \pm 0.7$	$37.3 \pm 1.1$
				$F = 2 \rightarrow 1$			

TABLE 2—*Continued*

Source	$\alpha$ (B1950.0)	$\delta$ (B1950.0)	Isotopomer	hf Component	$T_R^*$ (K)	$\Delta V_{1/2}$ (km s $^{-1}$ )	$V_{\text{LSR}}$ (km s $^{-1}$ )
SgrB2(OH) <sup>f</sup> .....	17 44 11.0	−28 22 30	CN	$F = 3/2 \rightarrow 1/2$	$\sim 1.2^{\text{g}}$	$\sim 9.6$	$\sim 57$
				$F = 5/2 \rightarrow 3/2$			
				$F = 1/2 \rightarrow 1/2$	$\sim 0.49^{\text{g}}$	$\sim 4.4$	$\sim 57$
				$F = 3/2 \rightarrow 3/2$	$\sim 0.19^{\text{g}}$	$\sim 5.2$	$\sim 57$
				$F = 1/2 \rightarrow 3/2$	$\sim 0.12^{\text{g}}$	$\sim 5.3$	$\sim 57$
			$^{13}\text{CN}$	$F = 3 \rightarrow 2$	$^{\text{g}}$	...	...
				$F = 2 \rightarrow 1$	$\sim 0.099^{\text{g}}$	$\sim 8.0$	$\sim 57$
				$F = 1 \rightarrow 0$	$\sim 0.048^{\text{g}}$	$\sim 10.1$	$\sim 57$
				$F = 2 \rightarrow 2$	$0.039 \pm 0.004^{\text{e}}$	$4.6 \pm 1.0$	$56.5 \pm 2.5$
				$F = 1 \rightarrow 1$			
Orion Bar <sup>a</sup> .....	05 32 53.5	−05 27 10	CN	$F = 3/2 \rightarrow 1/2$	$1.27 \pm 0.07$	$3.5 \pm 0.2$	$10.2 \pm 0.2$
				$F = 5/2 \rightarrow 3/2$	$3.62 \pm 0.07$	$3.4 \pm 0.1$	$10.3 \pm 0.3$
				$F = 1/2 \rightarrow 1/2$	$0.92 \pm 0.07$	$3.3 \pm 0.2$	$10.4 \pm 0.4$
				$F = 3/2 \rightarrow 3/2$	$0.96 \pm 0.06$	$3.6 \pm 0.2$	$10.2 \pm 0.2$
				$F = 1/2 \rightarrow 3/2$	$0.17 \pm 0.08$	$2.6 \pm 0.8$	$10.6 \pm 0.6$
			$^{13}\text{CN}$	$F = 3 \rightarrow 2$	$0.032 \pm 0.005$	$3.1 \pm 0.3$	$10.3 \pm 0.3$
				$F = 2 \rightarrow 1$	$0.022 \pm 0.007$	$2.9 \pm 0.3$	$10.3 \pm 0.3$
TMC-1 <sup>h</sup> .....	04 38 38.0	25 35 45	CN	$F = 3/2 \rightarrow 1/2$	$0.39 \pm 0.02$	$0.61 \pm 0.2$	$5.7 \pm 0.02$
				$F = 5/2 \rightarrow 3/2$	$0.22 \pm 0.02$	$0.66 \pm 0.3$	$5.6 \pm 0.01$
			$^{13}\text{CN}$	$F = 3 \rightarrow 2$	$0.028 \pm 0.006$	$0.8 \pm 0.2$	$5.8 \pm 0.1$
				$F = 2 \rightarrow 1$	$\leq 0.015$	...	...
L134N <sup>h</sup> .....	15 51 24.0	−02 43 31	CN	$F = 3/2 \rightarrow 1/2$	$0.13 \pm 0.02$	$0.5 \pm 0.2$	$2.6 \pm 0.01$
				$F = 5/2 \rightarrow 3/2$	$0.13 \pm 0.01$	$0.6 \pm 0.3$	$2.6 \pm 0.01$
			$^{13}\text{CN}$	$F = 3 \rightarrow 2$	$\leq 0.011$	...	...
				$F = 2 \rightarrow 1$	$\leq 0.011$	...	...

NOTE.—Errors are  $1\sigma$ , determined from Gaussian fits to the line profiles. Units of right ascension are hours, minutes, and seconds, and units of declination are degrees, arcminutes, and arcseconds.

<sup>a</sup> Observed with 500 kHz resolution.

<sup>b</sup> 3.5 km s $^{-1}$  component only.

<sup>c</sup> Blended with  $F = 5/2 \rightarrow 3/2$  line of the 12 km s $^{-1}$  component.

<sup>d</sup> Line self-reversed; intensity given for peak emission feature,  $V_{\text{LSR}}$  for self-absorption feature.

<sup>e</sup> Blended lines.

<sup>f</sup> Observed with 1 MHz resolution.

<sup>g</sup> Partially obscured by absorption feature.

<sup>h</sup> Observed with 100 kHz resolution.

emission lines at the correct frequencies, assuming  $V_{\text{LSR}} \sim 57$  km s $^{-1}$ —a typical velocity for this object (see, e.g., Nummelin et al. 2000).

## 5. ANALYSIS OF $^{12}\text{C}/^{13}\text{C}$ RATIOS

CN has a dipole moment of 1.5 D—considerably larger than that of CO (0.08 D). Consequently, even the  $N = 1 \rightarrow 0$  transition can only be excited in relatively dense gas ( $n \geq 10^3$  cm $^{-3}$ ), and thus large column densities, and large opacities, in this line might be expected. For Orion A and the Orion Bar, however, the hf components of CN show the optically thin, LTE intensity ratios. In W49, the hf components also indicate low optical depth, at least in the 4 km s $^{-1}$  component. (The 12 km s $^{-1}$  velocity component could not be evaluated because the main hf line at this velocity [ $F = 5/2 \rightarrow 3/2$ ] was unfortunately blended with the strong  $F = 3/2 \rightarrow 1/2$  component of the 4 km s $^{-1}$  component.) Therefore,  $^{12}\text{C}/^{13}\text{C}$  ratios were obtained for these objects by direct comparison of antenna temperatures of the main hf components of  $^{12}\text{CN}$  and  $^{13}\text{CN}$ , respectively ( $T_R^*$  of Table 2, using 500 kHz or 1 MHz data), corrected by the hf intensity ratio and for a small difference in beam efficiency.

For the other clouds investigated, larger opacities are present in  $^{12}\text{CN}$  ( $N = 1 \rightarrow 0$ ). Evaluation of the optical depth for each source was obtained by using a least-squares

analysis to simultaneously fit the ratios of the line intensities of at least four of the five hf components of  $^{12}\text{CN}$  to the general formula:

$$\frac{T_R^*(\text{hf})}{T_R^*(\text{main hf})} = \frac{1 - e^{-R_{\text{hf}}\tau_{\text{main}}}}{1 - e^{-\tau_{\text{main}}}}, \quad (1)$$

where  $T_R^*$  is the line temperature measured from the observed spectra,  $R_{\text{hf}}$  is the LTE intensity ratio of the given hf component to the main line ( $F = 5/2 \rightarrow 3/2$ ), and  $\tau_{\text{main}}$  is the optical depth in this line. For G34.3 and W33, the  $F = 1/2 \rightarrow 1/2$  component was not used in the fit because it was anomalously weak. Once  $\tau_{\text{main}}$  was established, an excitation temperature was then determined among the components using the expression

$$\frac{T_R^*}{\eta_c} = (T_{\text{ex}} - T_{\text{bg}})(1 - e^{-R_{\text{hf}}\tau_{\text{main}}}), \quad (2)$$

where  $\eta_c$  is the beam efficiency and  $T_{\text{bg}}$  is the cosmic background temperature ( $T_{\text{bg}} = 2.73$  K). The resulting opacities and excitation temperature are listed in Table 3. As shown in this table, most optical depths in the  $N = 1 \rightarrow 0$  transition were in the range  $\tau \sim 1.5$ – $5.2$ , where  $\tau = 3\tau_{\text{main}}$ , with  $T_{\text{ex}} \sim 6$ – $12$  K.

The opacities and excitation temperatures derived from this method were then used to predict the observed line

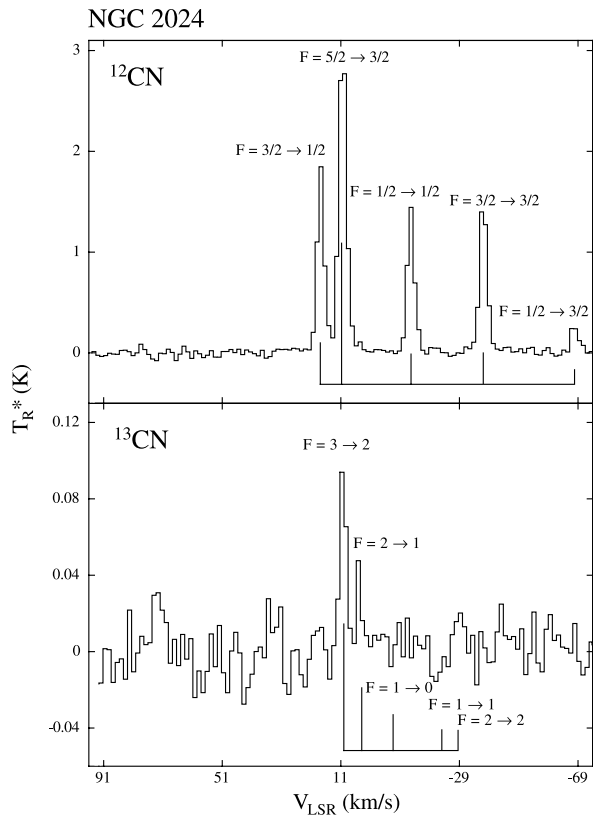


FIG. 1a

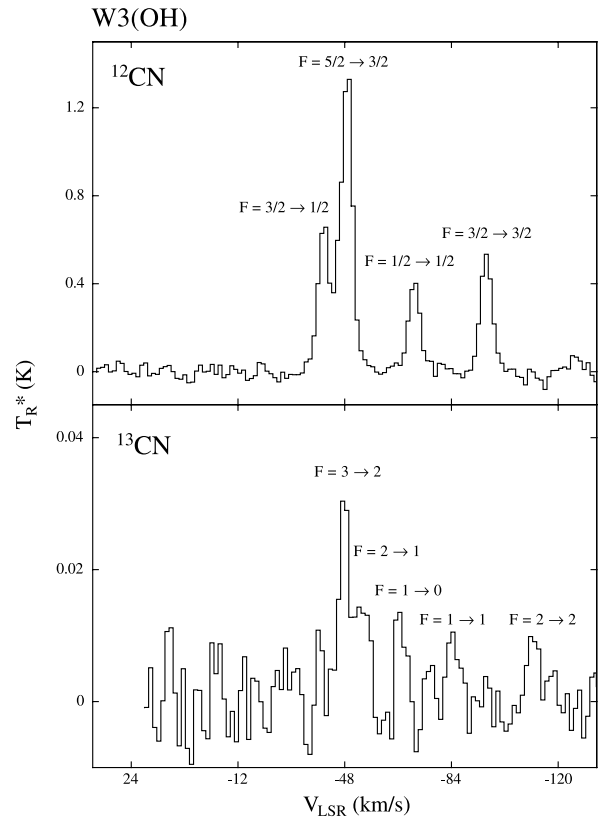


FIG. 1b

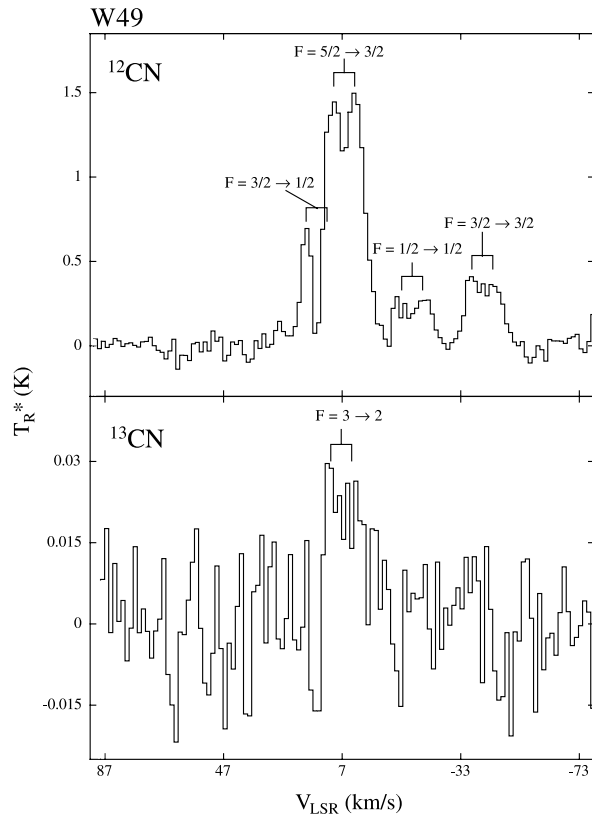


FIG. 1c

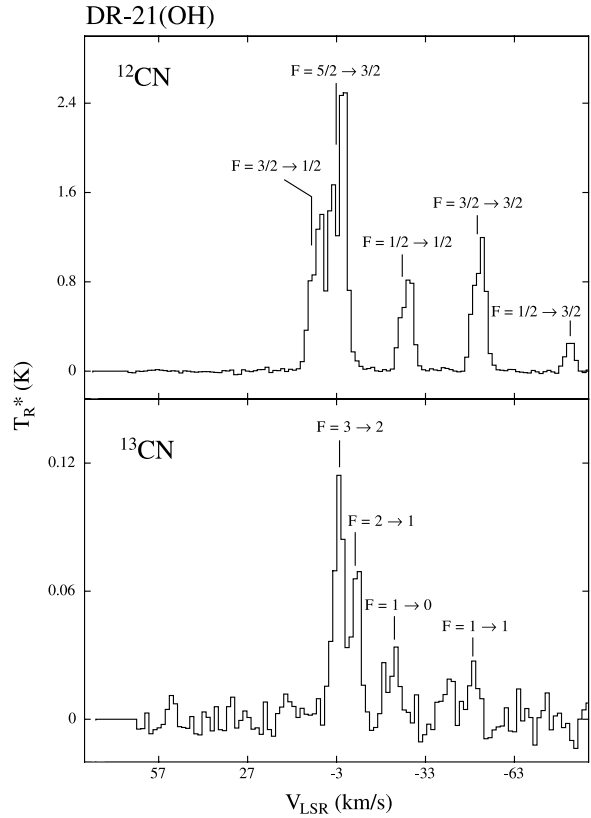


FIG. 1d

FIG. 1.—Spectra of the  $N = 1 \rightarrow 0$ ,  $J = 3/2 \rightarrow 1/2$  transition of  $^{12}\text{CN}$  (upper panels) and the  $N = 1 \rightarrow 0$ ,  $F_2 = 2 \rightarrow 1$  transition of  $^{13}\text{CN}$  (lower panels), observed with the Kitt Peak 12 m telescope. Filter-bank resolutions are given in Table 2. The CN hf structure and relative intensities are shown in (a) (NGC 2024). This hf structure has been used to accurately determine the optical depth in  $^{12}\text{CN}$  in order to evaluate  $^{12}\text{C}/^{13}\text{C}$  ratios.

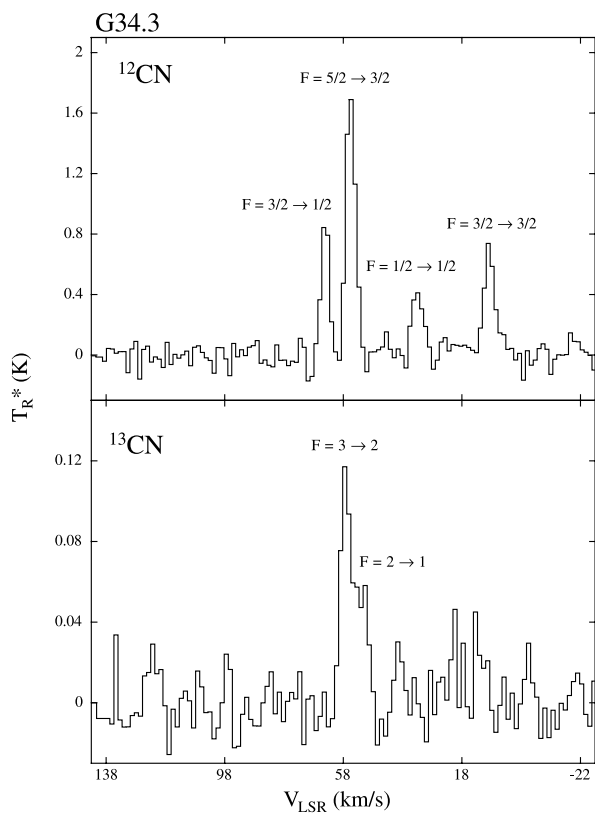


FIG. 1e

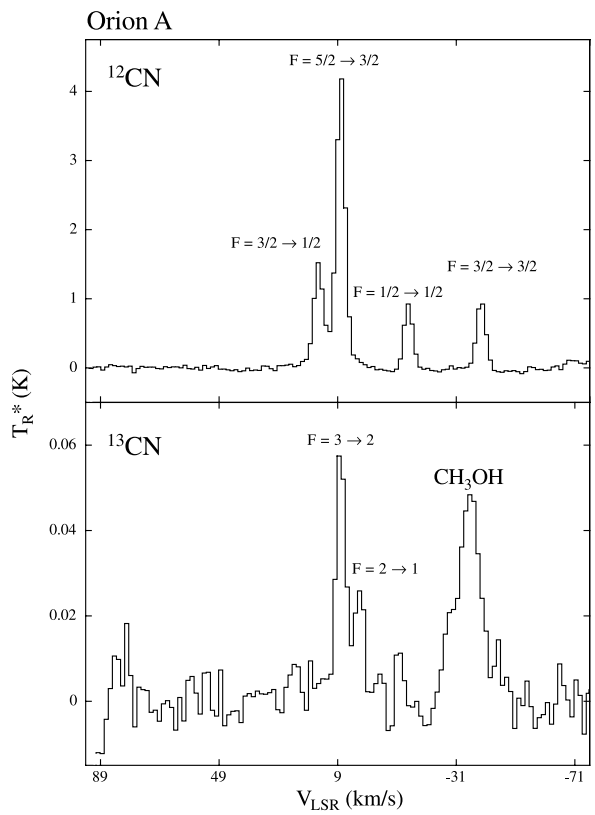


FIG. 1f

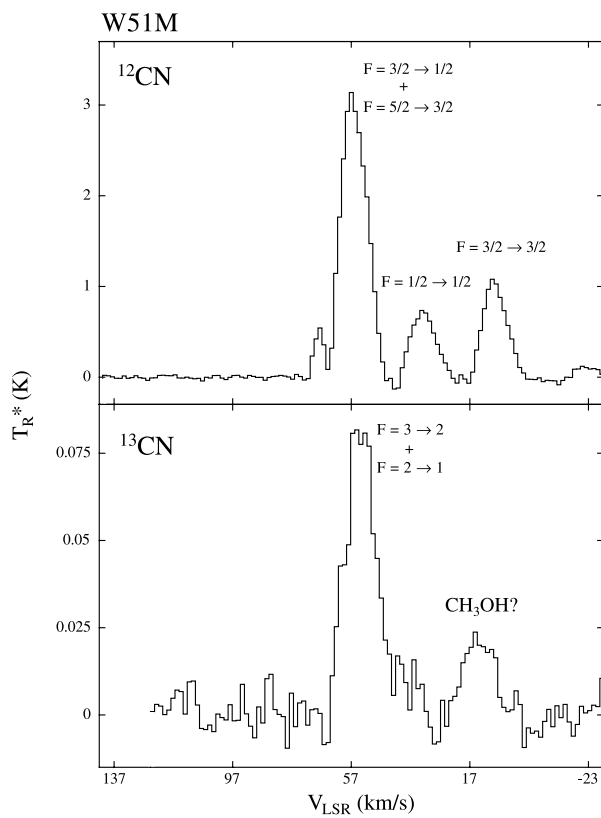


FIG. 1g

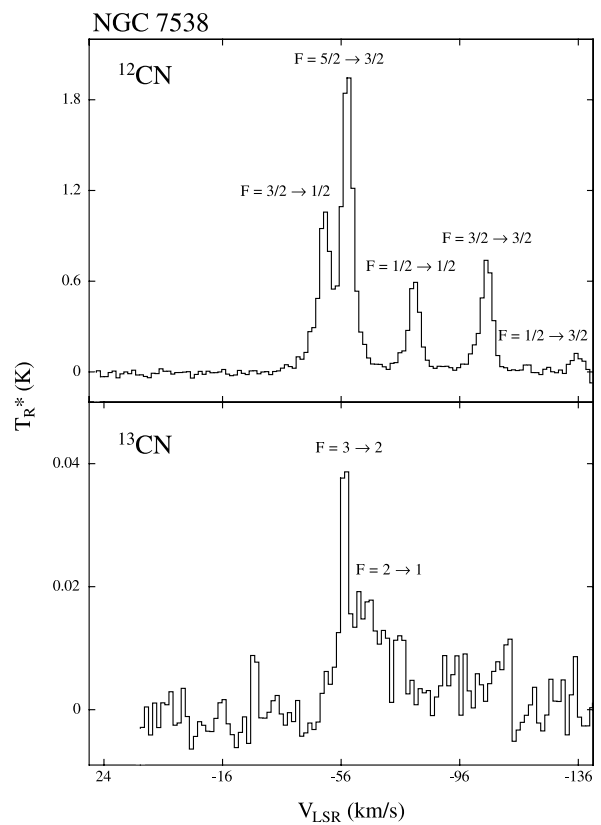


FIG. 1h

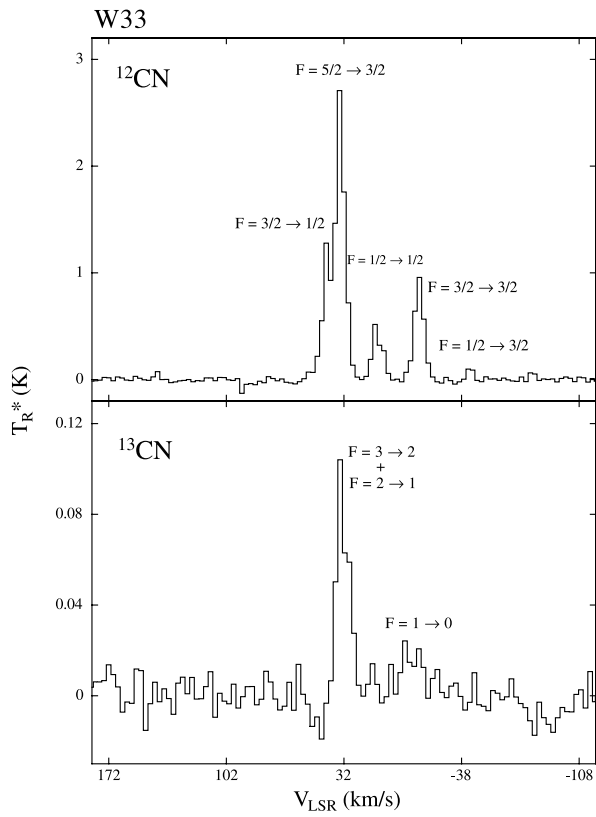


FIG. 1i

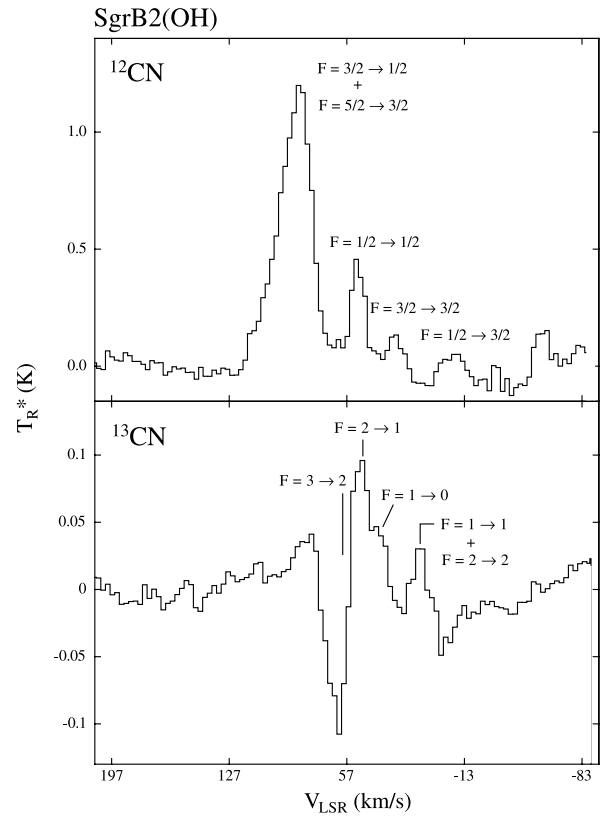


FIG. 1j

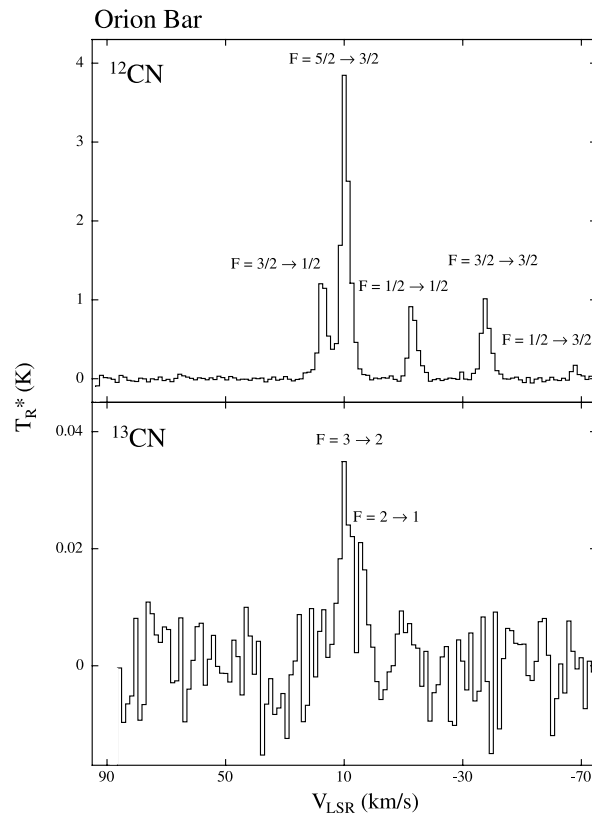


FIG. 1k

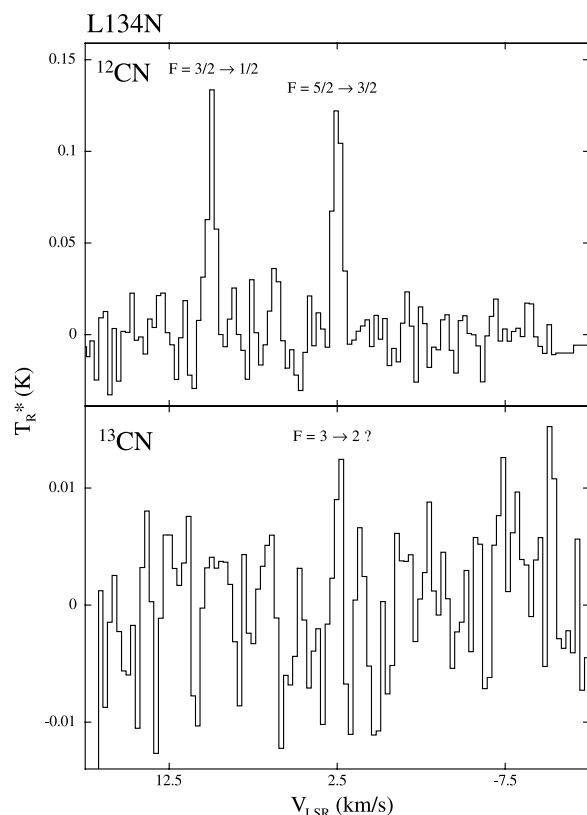


FIG. 1l

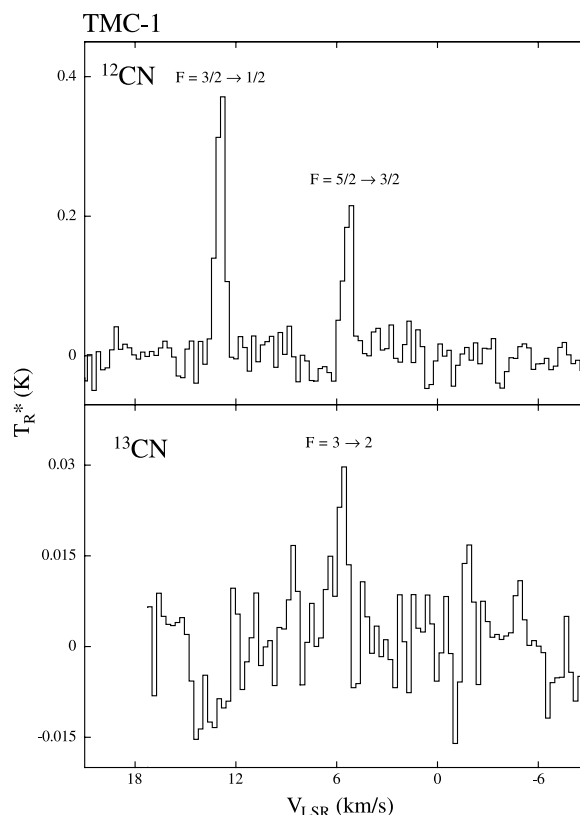


FIG. 1m

intensities for all hf components used in the fit, as an additional test of precision. All line intensities were reproduced to within an error of at worst 20%. Most components in fact were predicted to within a few percent. Thus, the slight deviation from LTE of the  $F = 1/2 \rightarrow 1/2$  hf component for sources such as W3(OH) and NGC 7538 did not significantly affect the overall data fits. The excitation temperature

in fact did not vary by more than  $\pm 1$  K and the opacity by  $\pm 0.3$  when comparing individual pairs of hf components.

Following these calculations, the  $^{12}\text{C}/^{13}\text{C}$  ratios were then determined using the following formula (in the Rayleigh-Jeans limit):

$$\frac{^{12}\text{C}}{^{13}\text{C}} = \frac{(3/5)\tau_{\text{main}}T_{\text{ex}}(^{12}\text{CN})}{T_R^*/\eta_c(^{13}\text{CN})}; \quad (3)$$

i.e.,  $\tau_{\text{main}}T_{\text{ex}}$  was used in place of the antenna temperature for the main hf component of  $^{12}\text{CN}$ . The  $^{13}\text{CN}$  line was assumed to be thin, as indicated by all observations, and  $T_R^*$  here applies to the intensity of the main hf component,  $F = 3 \rightarrow 2$  ( $F_2 = 2 \rightarrow 1$ ), of this species. The factor of  $\frac{3}{5}$  accounts for the relative intensities of the hf components for the two isotopomers (see Table 1). It is also assumed here that both CN isotopomers occupy the same volume, undergo the same degree of excitation, and are not subject to chemical anomalies.

There were a few sources where these direct methods could not be applied. These clouds were SgrB2(OH) and DR-21(OH), which exhibited some form of self-reversal. Consequently, for DR-21(OH), the weakest hf component of  $^{12}\text{CN}$  ( $F = 1/2 \rightarrow 3/2$ ) had to be used for the calculations (1.23% of the total intensity). This feature was chosen because it was sufficiently strong ( $T_R^* = 0.25$  K) and did not appear to be self-reversed. The antenna temperature of the  $F = 1/2 \rightarrow 3/2$  feature was compared to the main line of  $^{13}\text{CN}$ , under the optically thin assumption, as previously described. For SgrB2(OH), hf components had to be chosen that did not appear contaminated by absorption features. In the case of  $^{13}\text{CN}$ , absorption appeared to affect only the main hf component; hence, the  $F = 2 \rightarrow 2$  and  $F = 1 \rightarrow 1$

TABLE 3  
OPTICAL DEPTH AND COLUMN DENSITY OF  $^{12}\text{CN}$

Source	$\tau^a$	$T_{\text{ex}}$ (K)	$N_{\text{tot}}^b$ ( $\text{cm}^{-2}$ )
W3(OH).....	$1.9 \pm 0.4$	$6.0 \pm 0.5$	$3.6 \times 10^{14}$
W49 <sup>c</sup> .....	d	...	$2.6 \times 10^{14}$
DR-21(OH) <sup>e</sup> .....	...	...	$5.7 \times 10^{14}$
G34.3.....	$3.2 \pm 0.3$	$6.0 \pm 0.2$	$4.6 \times 10^{14}$
Orion A.....	d	...	$3.8 \times 10^{14}$
W51M.....	$1.5 \pm 0.5$	$12.4 \pm 2$	$1.3 \times 10^{15}$
NGC 7538.....	$1.8 \pm 0.2$	$8.1 \pm 0.5$	$4.4 \times 10^{14}$
NGC 2024.....	$5.2 \pm 0.2$	$7.3 \pm 0.1$	$7.9 \times 10^{14}$
W33.....	$2.2 \pm 0.2$	$8.9 \pm 0.4$	$8.6 \times 10^{14}$
SgrB2(OH).....	d	...	$4.1 \times 10^{14}$
Orion Bar.....	d	...	$3.0 \times 10^{14}$

NOTE.—Errors are  $1\sigma$ .

<sup>a</sup>  $\tau$  is the total optical depth in the  $N = 1 \rightarrow 0$  transition, i.e.,

$\tau = 3\tau_{\text{main}}$ .

<sup>b</sup> Assumed rotational temperature of 25 K.

<sup>c</sup>  $3.5 \text{ km s}^{-1}$  component.

<sup>d</sup>  $^{12}\text{CN}$  is optically thin;  $N_{\text{tot}}$  calculated in the thin limit.

<sup>e</sup> Column density calculated with  $F = 1/2 \rightarrow 3/2$  component, in the thin approximation.

lines were used for the ratio calculation. The latter two lines compose 7.2% of the total intensity of the  $N = 1 \rightarrow 0$  line of the  $^{13}\text{CN}$  isotopomer. For  $^{12}\text{CN}$ , all hf components appeared to have some evidence of absorption; the weakest hf feature,  $F = 1/2 \rightarrow 3/2$ , was employed for the ratio calculations since it seemed least contaminated, and the thin assumption was used. The value derived for SgrB2(OH) is thus a lower limit.

For the two dark clouds studied,  $^{12}\text{C}/^{13}\text{C}$  ratios were not determined. In TMC-1, the two hf lines observed exhibit a nonthermal intensity ratio. Therefore, any attempt to establish an isotope ratio would be highly uncertain. For L134N, the two hf components are sufficiently close in intensity that their ratio is no longer a sensitive indicator of optical depth. Hence, establishing an accurate opacity is also not realistic. Furthermore,  $^{13}\text{CN}$  was not conclusively detected in this source.

Also given in Table 3 are column densities calculated for  $^{12}\text{CN}$  based on the main hf component. These values were derived assuming a rotational temperature ( $T_{\text{rot}}$ ) of 25 K and using the formula (in the optically thin case)

$$N_{\text{tot}} = \frac{\zeta_{\text{rot}} 3k10^5 T_R \Delta V_{1/2}}{8\pi^3 \nu u_0^2 R_{\text{hf}}} . \quad (4)$$

In this expression,  $T_R$  is the beam-corrected antenna temperature,  $u_0^2$  is the dipole moment  $\zeta_{\text{rot}}$  is the rotational partition function, and  $\nu$  is the frequency of the  $N = 1 \rightarrow 0$  transition. For the optically thick sources,  $T_R$  is replaced by  $\tau_{\text{main}} T_{\text{ex}}$ . The column densities derived are in reasonable agreement with those determined from past millimeter-wave observations of CN (see, e.g., Churchwell 1980).

## 6. DISCUSSION

### 6.1. $^{12}\text{C}/^{13}\text{C}$ Ratios in the Galaxy

The  $^{12}\text{C}/^{13}\text{C}$  isotope ratios determined from the CN observations for all sources are presented in Table 4 along with Galactocentric distances. As the table shows, the ratios fall in the range 18–70. The lower ratios are

TABLE 4  
 $^{12}\text{C}/^{13}\text{C}$  RATIOS AND SOURCE GALACTOCENTRIC DISTANCES

Source	CN Ratio <sup>a</sup>	CO Ratio	H <sub>2</sub> CO Ratio	$D_{\text{GC}}$ (kpc)
W3(OH).....	63 ± 16	66 ± 4 <sup>b</sup>	91 ± 16 <sup>c</sup>	9.6
W49 <sup>d</sup> .....	44 ± 22	49 ± 6 <sup>b</sup>	53 ± 8 <sup>e</sup>	7.8
DR-21(OH) .....	36 ± 3	53 ± 2 <sup>b</sup>	...	8.0
G34.3 .....	28 ± 4	...	58 ± 5 <sup>e</sup>	5.2
Orion A.....	43 ± 7	67 ± 3 <sup>b,f</sup>	...	8.3
W51M .....	35 ± 12	45 ± 2 <sup>b</sup>	...	6.3
NGC 7538.....	56 ± 10	...	...	8.9
NGC 2024.....	65 ± 12	...	68 ± 11 <sup>c</sup>	8.3
W33.....	37 ± 8	39 ± 1 <sup>b</sup>	74 ± 11 <sup>c</sup>	4.1
SgrB2(OH).....	≥18 <sub>-6</sub>	24 ± 1 <sup>b</sup>	...	0.1
Orion Bar.....	70 ± 11	75 ± 9 <sup>g</sup>	...	8.3

<sup>a</sup> Errors are 1  $\sigma$ .

<sup>b</sup> Langer & Penzias 1990.

<sup>c</sup> Henkel et al. 1982.

<sup>d</sup> 3.5 km s<sup>-1</sup> component.

<sup>e</sup> Henkel et al. 1985.

<sup>f</sup> Langer & Penzias 1993 give 63 ± 6 at Orion A (-2.5, -14).

<sup>g</sup> Keene et al. 1998.

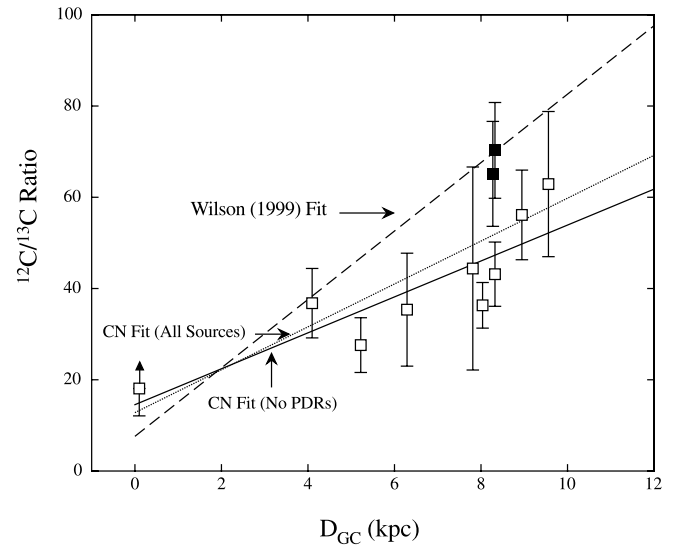


FIG. 2.— $^{12}\text{C}/^{13}\text{C}$  ratios for molecular clouds, determined from the CN observations, as a function of distance from the Galactic center. Two fits to these data are displayed on the plot, one that includes all sources and another that omits the two PDRs, NGC 2024 and the Orion Bar, which are shown as filled as opposed to open squares. Also shown is the fit derived from CO and H<sub>2</sub>CO measurements from Wilson (1999).

typically found for sources closer to the Galactic center [SgrB2(OH), W33, and G34.3]. In fact, the upper limit to the ratio for SgrB2(OH),  $^{12}\text{C}/^{13}\text{C} \geq 18$ , is in good agreement with the previously reported value for the Galactic center,  $^{12}\text{C}/^{13}\text{C} \sim 20$  (Wilson 1999). The average ratio for sources around the solar neighborhood (Orion A, NGC 2024, and the Orion Bar) is  $59 \pm 18$ , somewhat lower than the typical local ISM value of  $69 \pm 6$  (Wilson 1999) but certainly comparable within the quoted errors. However, NGC 2024 and the Orion Bar may not be representative of the local ISM since they are both photon-dominated regions (PDRs), as discussed later. The highest ratio in this study is found for the Orion Bar ( $70 \pm 11$ ), for example. None of the sources, however, exhibit ratios close to the solar system value of 89.

In Figure 2, the  $^{12}\text{C}/^{13}\text{C}$  ratio values are plotted against Galactocentric distance. As this graph shows, there appears to be a significant increase in the  $^{12}\text{C}/^{13}\text{C}$  ratio as the distance from the Galactic center increases. This effect has been well documented in other isotope studies, including  $^{14}\text{N}/^{15}\text{N}$  and  $^{16}\text{O}/^{18}\text{O}$  as well as  $^{12}\text{C}/^{13}\text{C}$  (see Wilson 1999). For CN, the increase in ratio values becomes significant at  $D_{\text{GC}} \geq 8$  kpc. [The SgrB2(OH) point is only a lower limit.] Part of this increase occurs because the two PDR sources, the Orion Bar and NGC 2024, lie at  $D_{\text{GC}} \sim 8.3$  kpc, and their ratios are high. Two other more “normal” sources, NGC 7538 and W3(OH), however, exhibit larger ratios as well. Interestingly, there does not appear to be a particularly obvious systematic increase in the  $^{12}\text{C}/^{13}\text{C}$  ratio between 4 and 8 kpc.

An unweighted least-squares fit to the CN data for all clouds yields the relationship

$$\frac{^{12}\text{C}}{^{13}\text{C}} = (4.7 \pm 1.3)D_{\text{GC}} + (12.8 \pm 8.5) , \quad (5)$$

which is plotted in Figure 2. If the two PDR sources are

neglected, then the fit obtained is (also see Fig. 2)

$$\frac{^{12}\text{C}}{^{13}\text{C}} = (3.9 \pm 0.9)D_{\text{GC}} + (14.5 \pm 6.3). \quad (6)$$

Both these expressions are somewhat different from that obtained by Wilson (1999), who fitted ratios from both CO and  $\text{H}_2\text{CO}$ . He obtained a slope of  $7.5 \pm 1.9$  and a  $y$ -intercept of  $7.6 \pm 12.9$ . This relationship is also plotted on Figure 2. The CN data fit is actually closer to the relationship obtained from CO measurements alone (Langer & Penzias 1993):

$$\frac{^{12}\text{C}}{^{13}\text{C}} = 6.0D_{\text{GC}} - 0.4. \quad (7)$$

The CO data, on the other hand, show a more systematic increase with  $D_{\text{GC}}$  over the range 4–8 kpc than CN, but these points are less consistent with the value obtained near the Galactic center (Langer & Penzias 1990).

### 6.2. Comparison with Measurements from Other Molecules

Additionally presented in Table 4 are  $^{12}\text{C}/^{13}\text{C}$  ratios obtained from CO and  $\text{H}_2\text{CO}$  (Langer & Penzias 1990, 1993; Henkel et al. 1982, 1985; Keene et al. 1998) for the same sources. As illustrated in these data, the ratios derived from CN are typically in close agreement with those obtained from CO. For example, the values from CN in W3(OH), W49, W33, SgrB2(OH), W51, and the Orion Bar are  $63 \pm 16$ ,  $44 \pm 22$ ,  $37 \pm 8$ ,  $\geq 18_{-6}$ ,  $35 \pm 12$ , and  $70 \pm 11$ , respectively. In comparison, those of CO are  $66 \pm 4$ ,  $49 \pm 6$ ,  $39 \pm 1$ ,  $24 \pm 1$ ,  $45 \pm 2$ , and  $75 \pm 9$  (Langer & Penzias 1990; Keene et al. 1998). In fact, the agreement is quite remarkable, given the different methods of analysis.

There are two sources where the ratios from CO and CN are different: DR-21(OH) (CN:  $37 \pm 4$ , CO:  $53 \pm 2$ ) and Orion A (CN:  $43 \pm 7$ , CO:  $67 \pm 3$ ). The DR-21(OH) value, however, had to be estimated from line profiles that, for the most part, were self-reversed. Hence, the  $^{12}\text{C}/^{13}\text{C}$  ratio may be underestimated. Self-reversal is not apparent in the CO data (Langer & Penzias 1990). In the case of Orion A, the situation is even more complicated because CO has multiple velocity components in this region and may be undergoing the chemical effects of shocks and star formation (Langer & Penzias 1990). In fact, the ratio listed for Orion A in CO was measured at a position (0'5, 2'5) from Orion KL, an area thought to be unaffected by the IRc2/BN outflows (Langer & Penzias 1990). The KL ratio itself is much higher:  $^{12}\text{C}/^{13}\text{C} = 79 \pm 7$ . CN, in contrast, exhibits only narrow, single-component line profiles near Orion KL and appears to exclusively arise from the ambient, extended ridge gas. Hence, it does not participate in the complicated chemistry of the IRc2/BN region. Therefore, it may be difficult to directly compare ratios obtained from CO and CN near Orion KL because they may not be arising from the same gas. It should be noted that in the PDR the Orion Bar, the ratios agree quite well; PDR chemistry may be affecting CO and CN similarly.

While there is good agreement between ratios determined from CO and CN, those established from  $\text{H}_2\text{CO}$  are significantly higher in every source studied. For example, in W3(OH), the value obtained from  $\text{H}_2\text{CO}$  is  $91 \pm 16$  versus  $63 \pm 16$  (CN) and  $66 \pm 4$  (CO). Another example is W33, where  $\text{H}_2\text{CO}$  yields  $^{12}\text{C}/^{13}\text{C} = 74 \pm 11$ , in contrast to  $37 \pm 8$  (CN) and  $39 \pm 1$  (CO). The ratios are also higher for

W49 and G34.3. The only cloud where the CN and  $\text{H}_2\text{CO}$  isotope ratio is comparable is NGC 2024 (Orion B), a well-known, face-on PDR (Schenewerk et al. 1988).

Another interesting comparison is between  $^{12}\text{C}/^{13}\text{C}$  ratios obtained from optical measurements of CN and radio observations. Unfortunately, optical studies of CN have only been conducted toward  $\zeta$  Oph, which is near the solar neighborhood. Although this ratio has been subject to many revisions (see, e.g., Hawkins et al. 1993; Crane & Hegyi 1988), the most current value is  $35 \pm 13$ , determined by Roth & Meyer (1995). This ratio may be characteristic of CN in the local ISM. It is in very good agreement with the radio CN value near a local cloud, Orion A ( $43 \pm 7$ ). (NGC 2024 and the Orion Bar are also in the local neighborhood, but they are both PDRs, and thus, any ratios determined in these objects may be subject to isotope-selective photo-dissociation, as will be further discussed.)

### 6.3. Chemical Fractionation of CN?

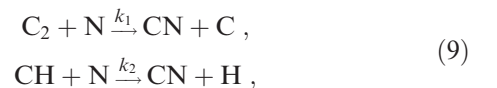
According to the early works of Watson et al. (1976), CO may be subject to chemical fractionation resulting from differences in zero-point energies of the  $^{12}\text{C}$  and  $^{13}\text{C}$  isotopomers, which is  $\sim 35$  K. Hence, carbon isotope ratios may be heavily weighted in favor of  $^{13}\text{C}$ , as given by the formula

$$\left(\frac{^{12}\text{C}}{^{13}\text{C}}\right)_{\text{measured}} = \left(\frac{^{12}\text{C}}{^{13}\text{C}}\right)_{\text{actual}} \exp\left(\frac{-35}{T_{\text{kin}}}\right). \quad (8)$$

However, as discussed by Wilson (1999), such fractionation effects cannot be too large because ISM values are within a factor of 2 of the solar system ratio of 89. In addition, a comparison can be made with  $\text{CH}^+$ —a molecule thought to be produced only by high-temperature (shock) processes and therefore not subject to chemical fractionation (Watson et al. 1976).  $\text{CH}^+$  thus far has only been studied via its optical electronic transitions. The local  $^{12}\text{C}/^{13}\text{C}$  ratio established from  $\text{CH}^+$  measurements is  $67 \pm 3$  (Centurión et al. 1995), in very good agreement with the local value obtained from CO of  $62 \pm 4$  (Langer & Penzias 1993). Chemical fractionation may not be playing an important role because typical molecular clouds have star formation and thus have gas kinetic temperatures higher than 35 K.

CN has been found to have a similar zero-point energy difference of 34 K for its  $^{12}\text{C}$  and  $^{13}\text{C}$  isotopomers (Kaiser et al. 1991). Consequently, it might be expected to undergo fractionation similar in magnitude to CO. However, as discussed by Langer et al. (1984), if CO is fractionated and the  $^{13}\text{C}$  isotopomer is enhanced, molecules formed from carbon monoxide will be  $^{12}\text{C}$ -enriched; i.e., the carbon-13 becomes “locked up” in  $^{13}\text{CO}$ , so it is not available for other species. If the Langer et al. theory is correct, then CN should only exhibit chemical fractionation if its synthesis is independent of CO.

Federman et al. (1994) have examined the production of interstellar CN and suggest that the major pathways to this molecule are



where  $k_1 \sim k_2 \sim 2.5 \times 10^{-11} \text{ cm}^3 \text{ s}^{-1}$ . The major precursors therefore are  $\text{C}_2$  and  $\text{CH}$ . A survey of the UMIST chemical reaction tables (Le Teuff, Millar, & Markwick 2000) concurs with these findings, except that there is a slight

temperature dependence of the reaction rates. These tables also indicate that  $C + NH$  and  $C + NO$  may be comparably fast routes to CN, although NH and NO are probably not as abundant as  $C_2$  and CH (see Halfen, Apponi, & Ziurys 2001). CN is primarily destroyed by reactions with N atoms:



where  $k_3 \sim 3 \times 10^{-10} \text{ cm}^3 \text{ s}^{-1}$ . Another destruction path is  $O + CN \rightarrow CO + N$ , but this reaction is about an order of magnitude slower than that involving N atoms. Consequently, at least to a first-order approximation, the reaction pathways leading to CN do not involve CO, although the opposite is possible.

The formation of CH and  $C_2$  also appears not to be directly linked to CO. CH is formed via the radiative association of  $C + H$  or from  $CH_2$ .  $C_2$  is synthesized from CH (Le Teuff et al. 2000). Therefore, the chemistry of CN cannot be influenced by CO through its major precursors. It is thus plausible that CN undergoes  $^{13}\text{C}$  enrichment comparable to (or even greater than) that of CO.

#### 6.4. Isotope-selective Photodissociation in Photon-dominated Regions

The highest carbon isotope ratios derived from CN occur toward the Orion Bar ( $70 \pm 11$ ) and NGC 2024 ( $65 \pm 11$ ). These two clouds are known PDRs, and CN is thought to be readily produced by the UV-induced chemistry of these objects (Sternberg & Dalgarno 1995). Observations have proven that CN is indeed abundant in PDR sources (see, e.g., Hogerheijde, Jansen, & van Dishoeck 1995; Fuente et al. 1993).

The presence of a large UV flux is thought to produce a “reverse” isotope effect. Molecules containing carbon-12 are more abundant than those with carbon-13; hence,  $^{12}\text{C}$  isotopomers are self-shielding and thus survive photodestruction better than their  $^{13}\text{C}$  counterparts. Thus,  $^{12}\text{C}/^{13}\text{C}$  ratios measured toward these objects may be  $^{12}\text{C}$ -enriched. Possible observational evidence has been found for such “isotope-selective photodissociation” in the Orion Bar. Isotope ratios derived from measurements of CI and  $C^+$  indicate  $^{12}\text{C}/^{13}\text{C} = 58 \pm 6$  (Boreiko & Betz 1996). Those determined from CO indicate  $^{12}\text{C}/^{13}\text{C} = 75 \pm 9$  (Keene et al. 1998).

The material composing the Orion A (or Orion KL) region lies approximately  $4'$  north of the Orion Bar, and basically these two sources are part of the same cloud complex. Isotope ratios should therefore be similar. To the contrary, for CN, the ratio in Orion A is  $43 \pm 7$ , while that in the Bar is  $70 \pm 11$ —a considerable increase. The CN ratio in the Bar is also much higher than the CI and  $C^+$  values. NGC 2024 (Orion B) is part of the local neighborhood as well, and the  $^{12}\text{C}/^{13}\text{C}$  ratio derived for this cloud is also high ( $65 \pm 11$ ), in comparison to the Orion A value. Isotope-selective dissociation is probably playing a significant role for CN in the Orion Bar and Orion B sources and enhancing the carbon ratio in favor of  $^{12}\text{C}$ .

#### 6.5. Implications for Chemical Evolution

These CN observations are additional evidence that significant chemical evolution has occurred, in both the solar neighborhood and the Galaxy. A useful comparison for the solar system is to examine comet isotope ratios. Optical observations of CN toward a sample of five recent comets yield an average value of  $^{12}\text{C}/^{13}\text{C} = 90 \pm 10$  (Wyckoff et al. 2000). All local clouds yield a much lower ratio from measurements of the same molecule. Consequently, if CN condensed directly from the primordial molecular cloud into solar system bodies such as comets, significant  $^{13}\text{C}$  enrichment (nearly a factor of 2) has occurred over the past 4.6 Gyr.

Our data also make the case for galactic evolution of the carbon isotope ratio quite compelling. The CN measurements confirm that a strong  $^{12}\text{C}/^{13}\text{C}$  gradient exists in the Galaxy. Clearly, secondary nucleosynthetic processes in low- and intermediate-mass stars have played a role in molecular cloud  $^{13}\text{C}$  enrichment as a function of both time and Galactic distance (see, e.g., Timmes et al. 1995; Boothroyd & Sackman 1999).

## 7. CONCLUSIONS

A new tracer has been used to establish  $^{12}\text{C}/^{13}\text{C}$  isotope ratios in dense Galactic molecular clouds: pure rotational transitions of interstellar CN. This molecule, although not as abundant as CO, is sufficiently prevalent that both the  $^{12}\text{C}$  and  $^{13}\text{C}$  isotopomers can be detected with reasonable integration times, therefore providing another independent constraint of this important ratio. Another advantage of CN measurements is that opacities in the  $^{12}\text{CN}$  lines can be evaluated from hf intensities. These observations suggest a  $^{12}\text{C}/^{13}\text{C}$  gradient in the Galaxy similar to CO and  $^{12}\text{C}/^{13}\text{C}$  ratios somewhat lower than average values obtained from combined CO and  $\text{H}_2\text{CO}$  data. Because the formation of CN is not linked to CO and the energy difference between its two carbon isotopomers is only 34 K, this molecule may undergo some chemical fractionation effects, comparable to those found in carbon monoxide. On the other hand, some evidence of  $^{12}\text{C}$  enrichment is found near two PDRs, probably caused by isotope-selective photodissociation. These ratios have also been compared with those determined from optical spectra of CN. While agreement is quite good in the solar neighborhood between the radio and optical values, the average  $^{12}\text{C}/^{13}\text{C}$  ratio derived from CN for a recent sample of comets is almost a factor of 2 larger. Substantial  $^{13}\text{C}$  enrichment appears to have occurred in the nearby ISM since the formation of the solar system.

This research is supported by NSF grant AST 98-20576. The authors thank John P. Schaefer and the Research Corporation for continued support of the Kitt Peak 12 m telescope, which enabled the completion of this project. C. S. thanks NASA for her graduate fellowship, and A. J. A. acknowledges the support of the National Italian-American Foundation.

## REFERENCES

- Anders, E., & Grevesse, N. 1989, *Geochim. Cosmochim. Acta*, 53, 197
- Blöcker, T. 1999, in *IAU Symp. 191, Asymptotic Giant Branch Stars*, ed. T. Le Bertre, A. Lébre, & T. Waelkens (Dordrecht: Kluwer), 21
- Bogey, M., Demuyneck, C., & Destombes, J. L. 1984, *Canadian J. Phys.*, 62, 1248
- Boothroyd, A. I., & Sackman, I.-J. 1999, *ApJ*, 510, 232
- Boreiko, R. T., & Betz, A. L. 1996, *ApJ*, 467, L113
- Centurión, M., Càssola, C., & Vladilo, G. 1995, *A&A*, 302, 243
- Churchwell, E. 1980, *ApJ*, 240, 811
- Crane, P., & Hegyi, D. J. 1988, *ApJ*, 326, L35
- Federman, S. R., Strom, C. J., Lambert, D. L., Cardelli, J. A., Smith, V. V., & Joseph, C. L. 1994, *ApJ*, 424, 772
- Fuente, A., Martín-Pintado, J., Cernicharo, J., & Bachiller, R. 1993, *A&A*, 276, 473
- Halfen, D. T., Apponi, A. J., & Ziurys, L. M. 2001, *ApJ*, 561, 244
- Hawkins, I., Craig, N., & Meyer, D. M. 1993, *ApJ*, 407, 185
- Henkel, C., Güsten, R., & Gardner, F. F. 1985, *A&A*, 143, 148
- Henkel, C., Wilson, T. L., & Bieging, J. 1982, *A&A*, 109, 344
- Hogerheijde, M. R., Jansen, D. J., & van Dishoeck, E. F. 1995, *A&A*, 294, 792
- Kaiser, M. E., Wright, E. L., & Hawkins, I. 1991, *ApJ*, 379, 267
- Keene, J., Schilke, P., Kooi, J., Lis, D. C., Mehringer, D. M., & Phillips, T. G. 1998, *ApJ*, 494, L107
- Lambert, D. L., Sheffer, Y., Gilliland, R. L., & Federman, S. R. 1994, *ApJ*, 420, 756
- Langer, W. D., Graedel, T. E., Frerking, M. A., & Armentrout, P. B. 1984, *ApJ*, 277, 581
- Langer, W. D., & Penzias, A. A. 1990, *ApJ*, 357, 477
- . 1993, *ApJ*, 408, 539
- Le Teuff, Y. H., Millar, T. J., & Markwick, A. J. 2000, *A&AS*, 146, 157
- Lucas, R., & Liszt, H. 1998, *A&A*, 337, 246
- Nummelin, A., Bergman, P., Hjalmarson, Å., Friberg, P., Irvine, W. M., Millar, T. J., Ohishi, M., & Saito, S. 2000, *ApJS*, 128, 213
- Richardson, K. J., White, G. J., Phillips, J. P., & Avery, L. W. 1986, *MNRAS*, 219, 167
- Roth, K. C., & Meyer, D. M. 1995, *ApJ*, 441, 129
- Schenewerk, M. S., Snyder, L. E., Hollis, J. M., Jewell, P. R., & Ziurys, L. M. 1988, *ApJ*, 328, 785
- Skatrud, D. D., de Lucia, F. C., Blake, G. A., & Sastry, K. V. L. N. 1983, *J. Mol. Spectrosc.*, 99, 35
- Sternberg, A., & Dalgarno, A. 1995, *ApJS*, 99, 565
- Timmes, F. X., Woosley, S. E., & Weaver, T. A. 1995, *ApJS*, 98, 617
- van Dishoeck, E. F., & Black, J. H. 1988, *ApJ*, 334, 771
- Watson, W. D., Anicich, V. G., & Huntress, W. T. 1976, *ApJ*, 205, L165
- Wilson, T. L. 1999, *Rep. Prog. Phys.*, 62, 143
- Wilson, T. L., & Rood, R. T. 1994, *ARA&A*, 32, 191
- Womack, M., Ziurys, L. M., & Wyckoff, S. 1992, *ApJ*, 387, 417
- Woosley, S. E., & Weaver, T. A. 1995, *ApJS*, 101, 181
- Wyckoff, S., Kleine, M., Peterson, B. A., Wehinger, P. A., & Ziurys, L. M. 2000, *ApJ*, 535, 991